5706 *Inorg. Chem.* **2010**, *49*, 5706–5714
DOI: 10.1021/ic100751a

Inorganic Chemistry
Article

Tuning Size and Thermal Hysteresis in Bistable Spin Crossover Nanoparticles

José Ramón Galán-Mascarós,*,† Eugenio Coronado,*,‡ Alicia Forment-Aliaga,‡ María Monrabal-Capilla,‡ Elena Pinilla-Cienfuegos,‡ and Marcelo Ceolin§

†*Institute of Chemical Research of Catalonia* (*ICIQ*), *Av. Paisos Catalans, 16, 43007 − Tarragona, Spain,* ‡*Instituto de Ciencia Molecular* (*ICMOL*), *Universidad de Valencia, Catedrático José Beltrán, 2, 46980 − Paterna, Spain, and* §*Instituto de Investigaciones Fisicoquímicas Teóricas y Aplicadas* (*UNLP-CONICET*), *Diagonal 113 y 64, 1900 − La Plata, Argentina*

Received April 19, 2010

Nanoparticles of iron(II) triazole salts have been prepared from water−organic microemulsions. The mean size of the nanoparticles can be tuned down to 6 nm in diameter, with a narrow size distribution. A sharp spin transition from the low spin (LS) to the high spin (HS) state is observed above room temperature, with a 30−40-K-wide thermal hysteresis. The same preparation can yield second generation nanoparticles containing molecular alloys by mixing triazole with triazole derivatives, or from metallic mixtures of iron(II) and zinc(II). In these nanoparticles of 10−15 nm, the spin transition "moves" towards lower temperatures, reaching a 316 K limit for the cooling down transition and maintaining a thermal hysteresis over 15−20-K-wide. The nanoparticles were characterized by dynamic light scattering, TEM, and AFM, after deposition on gold or silicon surfaces. The spin transition was characterized by magnetic susceptibility measurements and EXAFS (in solid samples after solvent removal) and also by the color change between the LS (violet) and HS (colorless) states in an organic solvent suspension. The discovery of bistable magnetic nanoparticles of 6 nm with a wide thermal hysteresis above room temperature showcases the actual possibilities of spin crossover materials for nanotechnological applications.

Introduction

Nanoparticles are acquiring the leading role in the search for miniaturization toward next generation devices, as several convenient methods are currently available for the preparation and manipulation of such nanomaterials. Magnetic nanoparticles are of particular interest due to the obvious data storage applications into high density media. In addition, functionalized magnetic nanoparticles can offer a wide variety of additional applications, specially for biological/medical usage.[1] Protein detection,[2] drug delivery,[3] or tumor treatment[4] are some other applications where magnetic nanoparticles can make a difference.

Current magnetic technologies are based on bulk magnets, but most of them will lose their properties of interest on the nanoscale, when the material cannot be considered as bulk anymore. In this context, molecular materials, where the property of interest resides in single molecules or in small arrays of molecules, could actually present a huge advantage. Coordination magnetic materials with technologically relevant magnetic properties have been already self-assembled from solution or by other soft processing methods into nanoparticles,[5] avoiding the use of expensive high-energy top-down physical methods of production. For instance, microemulsions or reverse micelles techniques have been used very successfully for the preparation of molecule-based nanoparticles with superparamagnetic[6,7] and photomagnetic[8,9] properties. The appearance of a magnetic "memory effect" is key in the search for magnetic nanoparticles to be integrated in actual devices, but unfortunately, bistability occurs at very low temperatures in most magnetic coordination compounds. The so-called spin crossover (SC) systems are one remarkable exception, one of the paradigmatic examples

*To whom correspondence should be addressed. Tel.: +34 977920808 (J.R.G.-M.), +34 963544415 (E.C.). Fax: +34 977920224 (J.R.G.-M.), +34 963543273 (E.C.). Web page: http://www.iciq.es/ (J.R.G.-M.), http://www.icmol.es/ (E.C.). E-mail: jrgalan@iciq.es (J.R.G.-M.), eugenio.coronado@uv.es (E.C.).

(1) Salata, O. V. *J. Nanobiotech.* **2004**, *2*, 3–8.
(2) Nam, J. M.; Thaxton, C. S.; Mirkin, C. A. *Science* **2003**, *301*, 1884–1886.
(3) Mah, C.; Zolotukhin, I.; Dobson, J.; Batich, C.; Byrne, B. J. *Mol. Therapy* **2000**, *1*, S239.
(4) Yoshida, J.; Kobayashi, T. *J. Magn. Magn. Mater.* **1999**, *194*, 176–184.
(5) Catala, L.; Volatron, F.; Brinzei, D.; Mallah, T. *Inorg. Chem.* **2009**, *48*, 3360–3370.
(6) Catala, L.; Gloter, A.; Stephan, O.; Rogez, G.; Mallah, T. *Chem. Commun.* **2006**, 1018–1020.
(7) Arai, M.; Miyake, M.; Yamada, M. *J. Phys. Chem.* **2008**, *112*, 1953–1962.
(8) Moore, J. G.; Lochmer, E. J.; Ramsey, C.; Dalal, N. S.; Stiegman, A. E. *Angew. Chem., Int. Ed.* **2003**, *42*, 2741–2743.
(9) Brinzei, D.; Catala, L.; Mathoniere, C.; Wernsdorfer, W.; Gloter, A.; Stephan, O.; Mallah, T. *J. Am. Chem. Soc.* **2007**, *129*, 3778–3779.

Published on Web 05/26/2010

of bistability at the molecular level.[10,11] In such transition metal complexes, a spin crossover between the low-spin (LS) configuration of the ground state and a metastable high-spin (HS) state can be triggered through external stimuli: thermally, via light irradiation, or under pressure.[12,13] The electronic transition accounts for several changes at the molecular level, affecting the metal−ligand distances (size) and optical properties (UV−vis absorption), in addition to magnetic properties. All of these possibilities have postulated SC systems as smart materials for information storage, molecular switching, sensing, and medical applications.[14,15]

The spin transition is of molecular origin, but the spin crossover phenomenon is strongly influenced by the surroundings in the crystal structure. While in solution one can observe a progressive monotonic population of the excited state, this process can become cooperative in the solid state, due to short- and long-range intermolecular interactions. Cooperativity usually gives rise to sharp spin transitions where all metal centers switch at the same time. In such cases, thermal hysteresis may also appear between the heating and cooling cycles, originating true bistability and a memory effect. Since this memory effect occurs in the bulk from the synergy between the SC process and a crystallographic phase transition, some controversy related to the size limit for spin crossover has started. If the memory effect disappears on the nanoscale, the possibilities for information storage media from SC systems will be clearly compromised, since they will not offer any improvement toward current technologies. Although some theoretical approximations have been used,[16] the complexity of the problem, depending on weak intermolecular interactions, precludes further predictions.

Several successful attempts to prepare spin crossover nanoparticles have been reported very recently. In all cases, the target compounds were polymeric iron(II) coordination complexes, since these materials usually show broad hysteresis close to room temperature. Nanoparticles of the [Fe(pyrazine)Pt(CN)$_4$] 3D network[17] (Figure 1) were prepared by Mallah et al. using reversed micelles, achieving size control by tuning the concentration of metal ions.[18] In this case, the remnant HS fraction of metal centers increases and the magnetic hysteresis decreases with the size of the nanoparticles. The hysteresis completely disappears around 7 nm diameter. Analogous results were found in parallel studies carried by Real et al. in nanoparticles of the same material, but following a different solid state treatment.[19] When [Fe(pyrazine)Pt(CN)$_4$] nanoparticles are stabilized into a biopolymeric matrix (chitosan), magnetic hysteresis is retained below 4 nm size, as demonstrated by

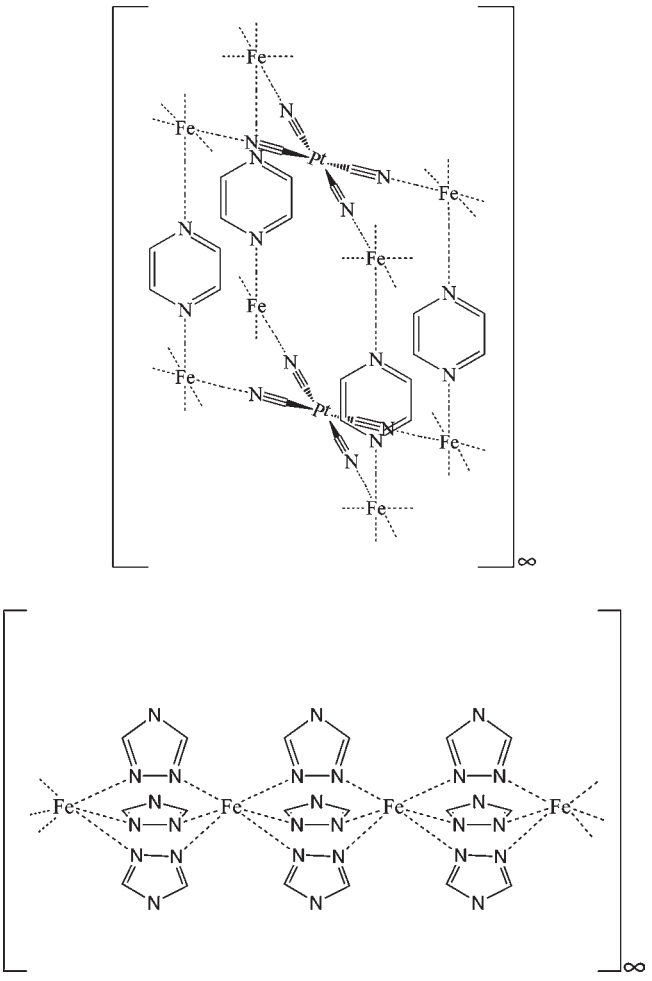

Figure 1. Molecular structure of polymeric spin crossover complexes: 3D [Fe(pyrazine)Pt(CN)$_4$]$_\infty$ (up) and 1D [Fe(trz)$_3$]$_\infty$ (down).

Bousseksou et al.,[20] although only about 1/3 of the iron(II) centers participate in the process. The decrease and further disappearance of the thermal hysteresis, and bistability, was related to the decrease in cooperativity when the iron atoms inside the nanoparticles start to be severely reduced compared with those on the surface.

Nanoparticles based on the [Fe(trz)$_3$]X$_2$ family[21] (trz = triazole) were reported independently by the group of Létard and by our research groups.[22,23] In these compounds, the metal ions are bound by the ligands giving 1D polymeric structures (Figure 1) that exhibit cooperative spin transition from Fe^{II} low spin (LS) to high spin (HS). In bulk materials, both, the temperature at which this transition occurs and the existence of a hysteresis during the process can be tuned by playing with combinations of different triazole derivatives or different anions.[24] The spin transition is associated in these

(10) Gütlich, P.; van Koningsbruggen, P. J.; Renz, F. *Struct. Bonding* (*Berlin*) **2004**, *107*, 27–75.
(11) Real, J. A.; Gaspar, A. B.; Muñoz, M. C. *Dalton Trans.* **2005**, 2062–2079.
(12) Gütlich, P. *Struct. Bonding* (*Berlin*) **1981**, *44*, 83–195.
(13) *Molecular Magnetism*; Kahn, O., Ed.; VCH Publishers: New York, 1993.
(14) Kahn, O.; Martinez, C. J. *Science* **1998**, *279*, 44–48.
(15) Gaspar, A. B.; Ksenofontov, V.; Seredyuk, M.; Gütlich, P. *Coord. Chem. Rev.* **2005**, *249*, 2661–2676.
(16) Kawamoto, T.; Abe, S. *Chem. Commun.* **2005**, 3933–3935.
(17) Niel, V.; Martínez-Agudo, J. M.; Muñoz, M. C.; Gaspar, A. B.; Real, J. A. *Inorg. Chem.* **2001**, *40*, 3838–3839.
(18) Volatron, F.; Catala, L.; Rivière, E.; Gloter, A.; Stéphan, O.; Mallah, T. *Inorg. Chem.* **2008**, *47*, 6584–6585.
(19) Boldog, I.; Gaspar, A. B.; Martínez, V.; Pardo-Ibáñez, P.; Ksenofontov, V.; Bhattacharjee, A.; Gütlich, P.; Real, J. A. *Angew. Chem.* **2008**, *47*, 6433–6437.
(20) Larionova, J.; Salmon, L.; Guari, Y.; Tokarev, A.; Molvinger, K.; Molnár, G.; Bousseksou, A. *Angew. Chem., Int. Ed.* **2008**, *47*, 8236–8240.
(21) Haasnoot, J. G. *Coord. Chem. Rev.* **2000**, *200*, 131–185.
(22) Létard, J.-F.; Nguyen, O.; Daro, N. PCT Int. Appl., CODEN: PIXXD2 WO 2007065996 A1 20070614 (in French), 2007.
(23) Coronado, E.; Galán-Mascarós, J. R.; Monrabal-Capilla, M.; García-Martínez, J.; Pardo-Ibáñez, P. *Adv. Mater.* **2007**, *19*, 1359–1361.
(24) (a) Kröber, J.; Codjovi, E.; Kahn, O.; Grolière, F.; MArtínez, C. J. *J. Am. Chem. Soc.* **1993**, *115*, 9810–9811. (b) Krober, J.; Audiere, J.-P.; Claude, R.; Codjovi, E.; Kahn, O. *Chem. Mater.* **1994**, *6*, 1404–1412. (c) Michalowicz, A.; Moscovici, J.; Ducourant, B.; Cracco, D.; Kahn, O. *Chem. Mater.* **1995**, *7*, 1833–1842.

triazole complexes with a significant color change, along with the change in the magnetic moment from $S_{LS} = 0$ to $S_{HS} = 2$. This color change, usually from deep purple/red to light pink or white, can be used to develop write/read applications. In the nanoparticles prepared following our synthetic procedure, we found an increase in the HS ratio, as in the past examples, but an almost unchanged thermal hysteresis for sizes as small as 10 nm in diameter. Surprisingly, nanoparticles of the analogous compound $[Fe(NH_2\text{-}trz)_3]Br_2 \cdot 3H_2O$ reported by Létard et al.,[25] exhibit disappearance of the thermal hysteresis when the size is decreased below 30 nm in diameter.[26]

Here, we report and confirm the possibility to prepare bistable nanoparticles from spin crossover complexes of iron(II) and triazole down to a few nanometers in size (~6 nm) maintaining an over 40 K thermal hysteresis. We also describe how to modulate the size and the magnetic properties playing with the chemical components of these nanoobjects. The size can be tuned by changing the ratio between solvents and surfactants. The magnetic hysteresis can be tuned by changing the chemical composition. Since our objective was to find nanoparticles showing bistability closer to room temperature, we tested molecular alloys by mixing 1,2,4-triazole with 4-amino-4H-1,2,4-triazole that were already successful for this purpose in bulk.[24] Finally, we also studied the effect of Zn doping on the magnetic properties of these nanoparticles.

Experimental Section

Synthesis. All chemicals and solvents used were of commercially available grade and were used without any previous purification. Bulk $[Fe(Htrz)_2(trz)](BF_4)$ was prepared by mixing stoichiometric amounts of $Fe(BF_4)_2 \cdot 6H_2O$ and 1,2,4-triazole in water. All synthetic procedures were done under an inert atmosphere.

Nanoparticles of $[Fe(Htrz)_2(trz)](BF_4)$. Sample **1**. A solution of $Fe(BF_4)_2 \cdot 6H_2O$ (1.0 g, 3.0 mmol) in water (6 mL) is added to a solution of sodium dioctylsulfosuccinate (10.0 g, 22.5 mmol) in *n*-octane (100 mL). After several minutes of stirring, this solution is filtered and transferred to a round-bottom flask containing behenic acid (2.0 g, 5.9 mmol). A solution of 1,2,4-triazole (0.6 g, 8.9 mmol) in ethanol (3 mL) is added to a solution of sodium dioctylsulfosuccinate (10.0 g, 22.5 mmol) in *n*-octane (100 mL). After several minutes of stirring, this solution is filtered and added to the previous solution. The mixture is stirred for 4 h and then centrifuged (3.000 rpm) and filtered to yield **1**.

Sample **2**. The same procedure as in sample **1** is used in this case, but using 15.0 g (33.7 mmol) of sodium dioctylsulfosuccinate in *n*-octane (100 mL) in each solution. In this case, the nanoparticles were centrifuged at 50.000 rpm.

Sample **3**. The same procedure as in sample **1** is used in this case, but using 20.0 g (44.9 mmol) of sodium dioctylsulfosuccinate in *n*-octane (100 mL) in each solution.

Nanoparticles of $[Fe(Htrz)_{3-x}(NH_2trz)_x](ClO_4)_2$. Sample **4** ($x = 0.05$). A solution of $Fe(ClO_4)_2 \cdot H_2O$ (1.0 g, 4.0 mmol) in water (6 mL) is added to a solution of sodium dioctylsulfosuccinate (10.0 g, 22.5 mmol) in *n*-octane (100 mL). After several minutes of stirring, this solution is filtered and transferred to a round-bottom flask containing behenic acid (2.0 g, 5.9 mmol). A solution of 1,2,4-triazole (0.80 g, 11.8 mmol) and 4-amino-4H-1,2,4-triazole (0.015 g, 0.2 mmol) in ethanol (3 mL) is added to a solution of sodium dioctylsulfosuccinate (10.0 g, 22.5 mmol) in *n*-octane (100 mL) with a small amount of L-ascorbic acid. After several minutes of stirring, this solution is filtered and added to the previous solution. The mixture is stirred for 4 h and then centrifuged (3000 rpm) and filtered to yield **4**.

Sample **5** ($x = 0.15$). The same procedure as in sample **4** is used in this case, but with 11.4 mmol of 1,2,4-triazole and 0. 6 mmol of 4-amino-4H-1,2,4-triazole.

Sample **6** ($x = 0.30$). The same procedure as in sample **4** is used in this case, but with 10.8 mmol of 1,2,4-triazole and 1.2 mmol of 4-amino-4H-1,2,4-triazole.

Nanoparticles of $[Fe_{0.8}Zn_{0.2}(Htrz)_2(trz)](BF_4)$. Sample **7**. The same procedure as in sample **1** is used in this case, but using 2.4 mmol of $Fe(BF_4)_2 \cdot 6H_2O$ and 0.6 mmol of $Zn(BF_4)_2 \cdot H_2O$.

Physical Characterization. Infrared spectra were obtained as KBr pellets on a Nicolet 5700 FT-IR spectrophotometer. Magnetic susceptibility measurements were performed on solid samples, after centrifugation/filtration of the *n*-octane suspensions. Magnetic data were collected with a Quantum Design MPMS-XL-5 susceptometer equipped with a SQUID sensor. Due to the impossibility to properly estimate the surfactant/solvent content, and since only the iron centers are paramagnetic in the sample, susceptibility data were normalized for complete HS population in the high temperature regime. Therefore, data were plotted per mol of Fe. DC static data were collected in the range 2−400 K with an applied field of 1000 or 5000 G (sample **2**). The heating−cooling cycles were done with a rate of 1−2 K per minute. Transmission electron microscopy (TEM) images were collected after solvent evaporation of droplets of the sample suspensions in *n*-octane on carbon-coated copper grids with a JEOL JEM-1010 microscope (100 kV) equipped with a MegaView III camera. Size distribution of the samples was determined by dynamic light scattering of a suspension in *n*-octane with a Marlvern Zetasizer instrument.

EXAFS Measurements. X-ray absorption spectroscopy data were collected in the D04B-XAFS1 experimental station of the National Synchrotron Light Laboratory, Campinas, Brazil. Sample preparation started by mixing about 5 mg of the sample with 10−15 mg of boron nitride. After gentle and careful mixing, the powder was compacted to less than 1 mm. Each individual run lasted about 30 min on the radiation beam, and typically, three independent frames were acquired for each sample. The experiments were performed using a Si(220) channel cut monochromator with a calculated energy resolution (at 7112 eV including experimental resolution and natural line width) of ~1.5 eV. Sample temperature was controlled to ±0.1 K. All experiments were performed in transmission mode using a metallic iron foil for energy calibration and individual spectra alignment. Data reduction and analysis were performed using the IFEFFIT package.[28]

Atomic Force Microscopy. On gold: A thermal annealing of the evaporated gold films was necessary to improve the flatness of the gold substrate producing atomically flat terraces. The sample was prepared by immersing the gold substrate into a diluted suspension of **1** in a mixture of *n*-octane for around 2 min. Then, the surface was first rinsed with *n*-octane and blown dry in N_2 gas and then with acetone and dried with N_2 gas again. The AFM images were performed in the tapping mode (AFM Multimode, Veeco) under ambient conditions, using silicon cantilevers (Veeco Probes) with a force constant of about 40 N m^{-1} and a resonance frequency around 320 kHz. On silicon: The silicon samples (p-type < 100 > from DXL enterprises, INC) were cleaned by sonication in organic solvents. In this case, the suspensions of **1** were dialyzed prior to the

(25) Forestier, T.; Mornet, S.; Daro, N.; Nishihara, T.; Mouri, S.-I.; Tanaka, K.; Fouché, O.; Freysz, E.; Létard, J.-F. *Chem. Commun.* **2008**, 4327–4328.

(26) Forestier, T.; Kaiba, A.; Pechev, S.; Denux, D.; Guionneau, P.; Etrillard, C.; Daro, N.; Freysz, E.; Letard, J.-F. *Chem.—Eur. J.* **2009**, *15*, 6122–6130.

(27) Kröber, J.; Codjovi, E.; Kahn, O.; Grolière, F.; Jay, C. *J. Am. Chem. Soc.* **1993**, *115*, 9810–9811.

(28) Newville, M. *J. Synchrotron. Radiat.* **2001**, *8*, 322–324.

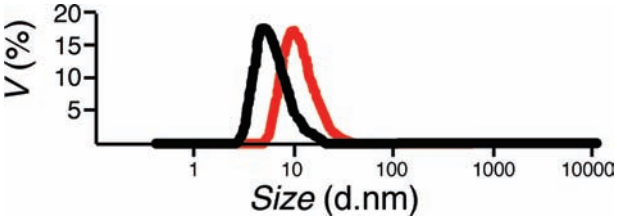

Figure 2. Volume ratio vs diameter size (logarithmic scale) for diluted suspensions in *n*-octane of samples 1 (red) and 2 (black).

deposition. The samples were prepared by immersing the silicon substrate into a diluted suspension of **1** in *n*-octane for a few seconds. Then, the substrate was immersed in pure *n*-octane and finally blown dry in N_2. The AFM images were performed in the tapping mode (AFM Multimode, Veeco) under ambient conditions, using silicon Super Sharp cantilevers (Veeco Probes) with a force constant of about 42 N m^{-1} and resonance frequency around 320 kHz.

Results and Discussion

The synthetic method we developed for the preparation of $[Fe(Htrz)_2(trz)](BF_4)$ nanoparticles was modified to study the changes in particle size by changing the ratio between solvents and surfactants. The general trend we expected of lower particle sizes by increasing the surfactant/solvent ratio was indeed observed. The smallest particle size we could regularly isolate had a mean 6 nm hydrodynamic diameter, according to dynamic light scattering (Figure 2). When a larger surfactant/solvent ratio was used in the search for smaller sizes, polycrystalline materials start to appear as the main product, with sizes larger than 1000 nm. Still, as in sample **3**, a small amount of nanoparticles between 35 and 50 nm was found.

After all our preparative studies, the role of behenic acid in the synthesis is still unclear. It could be involved in the formation of the micelles or as a coordinating agent stabilizing the surface of the nanoparticles. Indeed, the presence of behenic acid as part of the surfactant shell in the nanoparticles was confirmed by IR spectra (Figure S8, Supporting Information). The nanoparticles show a broad carbonyl band between 1700 and 1740 cm^{-1}, a combination of the two distinctive sharp carbonyl bands of behenic acid (close to 1700 cm^{-1}) and AOT (1735 cm^{-1}). Additionally, in the absence of behenic acid, no nanoparticles could be successfully isolated, with partial oxidation processes taking place and competing in the synthesis.

Two additional chemical strategies were used to modify the magnetic hysteresis without changing the particle size. The preparation process was identical in all cases, but mixtures of ligands or metal ions were used. We tested different mixed polymers of triazole with N-amino-triazole, and nanoparticles of controlled size were indeed obtained. We also doped the nanoparticles with different amounts of diamagnetic Zn^{2+} ions. These ions substitute the Fe^{2+} ions in the chain and essentially reduce the chain length/cooperativity for the spin crossover.

It is important to mention that no further treatment after synthesis and isolation was done to the samples. Therefore, the nanoparticles remain inside a bulky layer of surfactants. They can be suspended in *n*-octane or other nonpolar solvents and easily recovered through slow evaporation, without meaningful weight losses. Only the process of heating the solutions above reflux conditions produces surfactant loses in the nanoparticles, when a white precipitate appears.

Table 1. Size Analysis for Samples **1**−**7**

sample	stoichiometry	mean diameter size
1	$[Fe(Htrz)_2(trz)](BF_4)$	11 ± 5 nm
2	$[Fe(Htrz)_2(trz)](BF_4)$	6 ± 3 nm
3	$[Fe(Htrz)_2(trz)](BF_4)$	35 ± 6 nm; >1000 nm
4	$[Fe(Htrz_{2.95}(NH_2trz)_{0.05}](ClO_4)_2$	13 ± 6 nm
5	$[Fe(Htrz_{2.85}(NH_2trz)_{0.15}](ClO_4)_2$	12 ± 5 nm
6	$[Fe(Htrz_{2.70}(NH_2trz)_{0.30}](ClO_4)_2$	11 ± 5 nm
7	$[Fe_{0.8}Zn_{0.2}(Htrz)_2(trz)](BF_4)$	10 ± 4 nm

Still, the physical properties of the nanoparticles remain essentially unchanged throughout this process.

The particle size distribution for all samples was determined by dynamic light scattering (Supporting Information), and it is summarized in Table 1. This bulk analysis of the whole samples shows a narrow size distribution of the nanoparticles, proving the high selectivity of the preparative process.

These results are in good agreement with TEM images (Figure 3), which show a regular size distribution (∼15 ± 5 nm) and little tendency toward aggregation in *n*-octane suspensions. These nanoparticles were first isolated as a solid sample and later suspended in *n*-octane for electron microscopy. This supports once again the stability of the nanoparticles in time and through chemical treatment.

Magnetic Properties. The magnetic properties of **1** were already described previously.[26] These 11 ± 5 nm particles show a stable multicycle thermal hysteresis of 41 K ($T_c\uparrow$ = 384 K and $T_c\downarrow$ = 343 K) with a remnant HS ratio of about 20%. This HS ratio is more than double that found in the bulk, and it should be related to the higher surface area of nanoparticles. Surface Fe atoms will possess a partial coordination sphere, favoring their HS state at all temperatures.

When the particle size is reduced down to 6 ± 3 nm (**2**), the magnetic behavior starts to deviate from the bulk (Figure 4). A 29-K-wide hysteresis ($T_c\uparrow$ = 372 K and $T_c\downarrow$ = 343 K) is found in this case, with a higher remnant HS residue (∼33%), as expected for a smaller particle size. It is interesting to note that the temperature of the transition changes only in the heating cycle, while it remains identical in the cooling cycle. In both cases, the transition is still very sharp.

The magnetic properties for samples **4**−**6**, formed by mixtures of ligands (triazole and N-amino-triazole), show different features (Figures 5−7). As expected, the transition moves to lower temperatures in both cycles, heating and cooling. Sample **4** exhibits a stable 23 K hysteresis ($T_c\uparrow$ = 346 K and $T_c\downarrow$ = 323 K), after the first heating that occurs at 358 K. The displacement toward lower temperatures in the heating cycle is a typical behavior in all nanoparticles studied, as it was already observed in **1**. This only occurs in the first cycle, since all successive cycles are identical. A desolvation process should be responsible for this change. The slightly larger size of these nanoparticles is responsible for the lower remnant HS ratio at low temperatures (∼8%).

The trend indicates that the thermal hysteresis moves to lower temperatures and becomes narrower as the ratio of amino−triazole increases. Thus, sample **5** exhibits a stable 17 K hysteresis ($T_c\uparrow$ = 338 K and $T_c\downarrow$ = 321 K), and sample **6** exhibits a stable 28 K hysteresis ($T_c\uparrow$ = 344 K and $T_c\downarrow$ = 316 K). In this last case, the HS ratio increases dramatically.

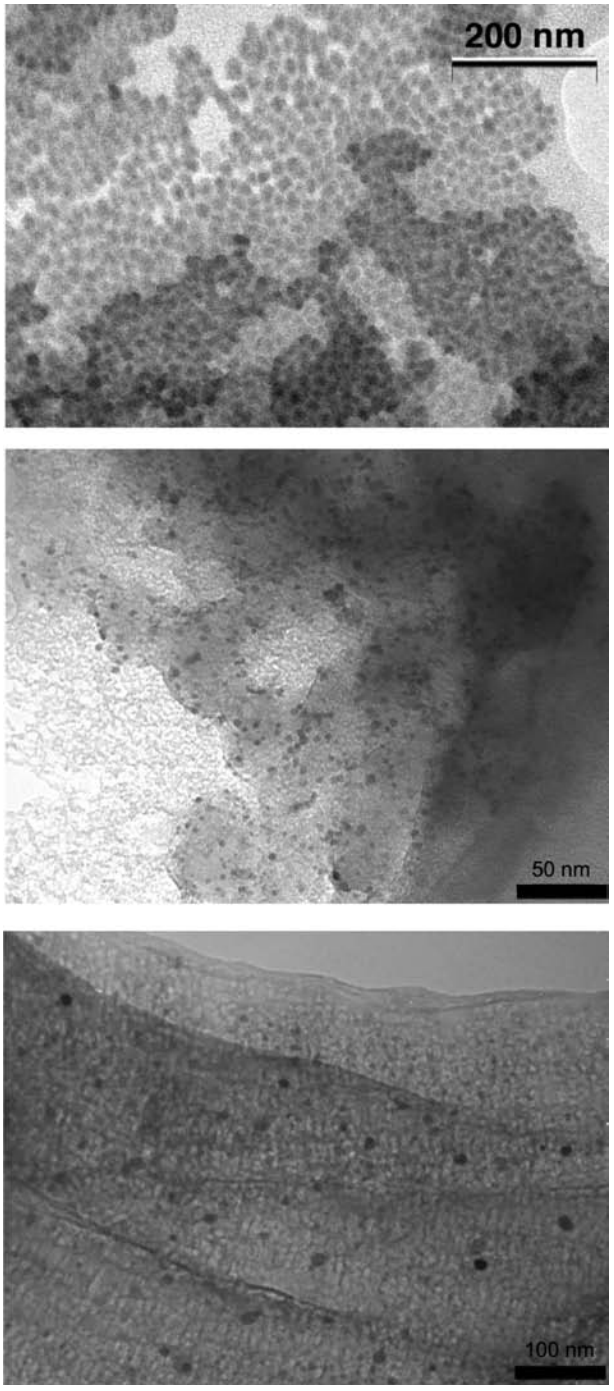

Figure 3. TEM images of **1** (up), **4** (center), and **7** (down).

Sample **7**, formed by a Fe/Zn mixture, shows a transition, although it is not as sharp as in other samples (Figure 8). In the heating process, the increase of the magnetic moment is very smooth between 330 and 360 K, where a jump appears up to saturation. Surprisingly, this does not occur in the cooling protocol, where a sharp transition is observed. This generates a 21 K hysteresis ($Tc\uparrow$ = 357 K and $Tc\downarrow$ = 336 K). This smooth behavior needs to be related to the random distribution of Zn atoms in the chains, cutting the length and cooperativity in the Fe−triazole chains in a random way.

All magnetic measurements were performed in solid dry samples, after filtration. We were not able to follow

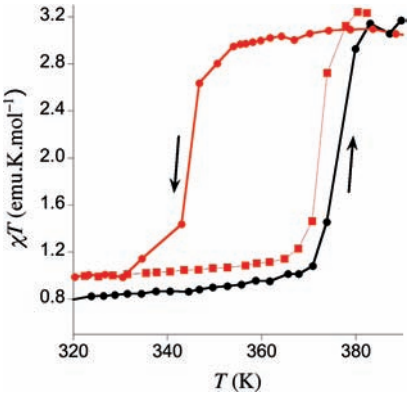

Figure 4. Temperature dependence of the magnetic moment for sample **2** (black circles, 1st heating protocol; red squares, stable hysteresis cycle).

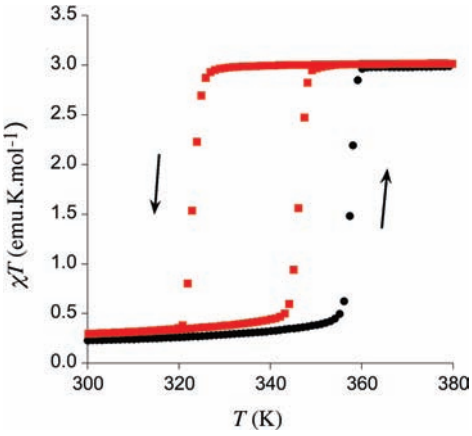

Figure 5. Temperature dependence of the magnetic moment for sample **4** (black circles, 1st heating protocol; red squares, stable hysteresis cycle).

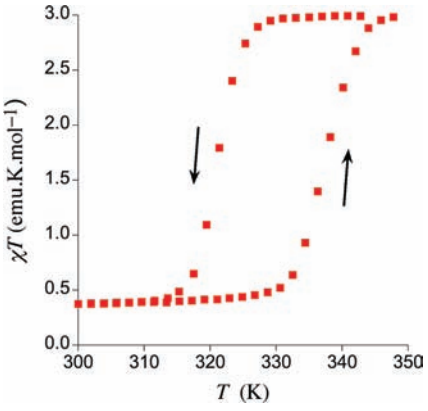

Figure 6. Temperature dependence of the magnetic moment for sample **5** after several heating−cooling cycles.

magnetically the spin transition in suspension, due to the difficulties in handling the liquid samples. Other techniques can be helpful in this regard, taking advantage of the multiple features of the spin transition. Actually, the thermal hysteresis in a suspension of **1** in n-octane can be followed with the naked eye through its color change (Figure 9) from the purple LS state to the colorless HS state. The pictures shown in Figure 9 have been extracted from a real time movie (Supporting Information) with the heating and cooling process of two identical suspensions of **1**. It is important to mention that another research

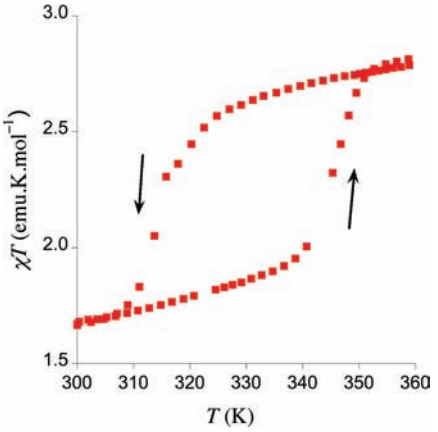

Figure 7. Temperature dependence of the magnetic moment for sample **6** after several heating−cooling cycles.

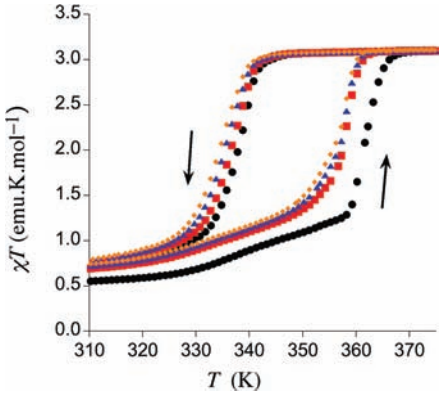

Figure 8. Temperature dependence of the magnetic moment for sample **7** (black circles, 1st cycle; red squares, 2nd cycle; blue triangles, 3rd cycle; orange circles, 4th cycle).

group, following the preparation described in our previous paper, has reproduced our results. In addition, they have been able to gather precise UV−vis spectra at multiple temperatures of nanoparticle suspensions.[28] Their results are identical to ours, confirming independently that the spin crossover occurs on the nanoscale in these materials, and that the thermal hysteresis still exists, at least down to a few nanometer sizes.

EXAFS. X-ray absorption experiments were performed in samples **1** and **2** and in a bulk sample of $[Fe(Htrz)_2(trz)](BF_4)$ in order to gain information about the iron charge state and local coordination, since the spin transition should affect these features. XANES spectra obtained for the low and high spin phases (Supporting Information) show small but noticeable changes in edge position around energies compatible with Fe^{II}. The k^2-weigthed EXAFS spectra (Supporting Information) display well-defined oscillations up to $k = 13$ Å^{-1}, suggesting an ordered coordination environment around iron. Fast Fourier transformation (FFT) of the k^2-weigthed EXAFS spectra (Figure 10) displays low Z elements coordinating iron. At room temperature, the coordination distance shows a mean value of 1.96 ± 0.01 Å. The same identical distance is found for the three different samples. These numbers are in good agreement with the LS state that shows shorter metal−ligand bonding. When the measurements were carried out at 397 K, there is an increase in the coordination distance of the Fe^{II} up to 2.19 ± 0.04 Å in the bulk. Analogous results are found for samples **1** and **2**, but with slightly shorter values of 2.17 ± 0.09 Å and 2.14 ± 0.01 Å, respectively. The only reasonable explanation for this change needs to be related to the particle size, and to the surface/core ratio. It was already determined that the surface Fe^{II} centers do not undergo any spin transition, and they remain in the HS state at all temperatures, because of the different coordination sphere. This different coordination sphere (containing carboxilate ligands) needs to be slightly shorter than the Fe−triazole distance. As the ratio of surface atoms increases, the average coordination distance for the HS Fe^{II} centers decreases. This, of course, does not affect the LS centers, since the transition only occurs in the core Fe^{II} atoms, with identical coordination in all samples, no matter the size.

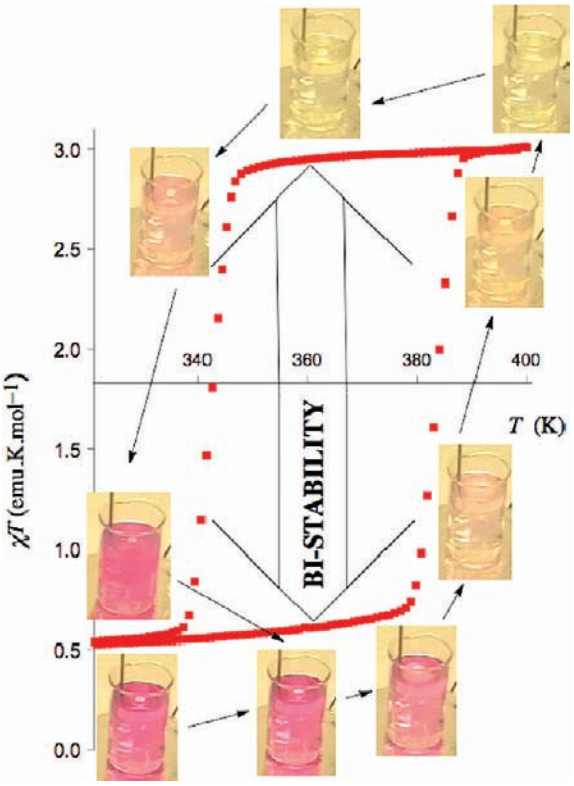

Figure 9. Thermal hysteresis in an *n*-octane suspension of sample **1**.

Surface Deposition and Atomic Force Microscopy. The nanoparticles described in this article, without further functionalization, show a tendency to be fixed onto gold or silicon surfaces, without significant aggregation. This feature allowed us to prepare gold or silicon surfaces covered with nanoparticles of **1**. In Figure 11, we show AFM images of gold covered surfaces. Although the nanoparticles tend to bind into the surface defects, many individual nanoparticles can be seen deposited on the flat areas. Images of single nanoparticles (Figure 12) are in very good agreement with the ∼5−15 nm diameter found by all other experiments. In addition, this close look shows that some nanoparticles are indeed forming couples.

In Figure 13, we show AFM images of nanoparticles of **1** on silicon surfaces. In this case, the nanoparticles are easily deposited uniformly on the flat regular surface. In addition, the compositional map of the phase image[29]

(29) Ph.D. Thesis defense of Victor Martínez (2009).

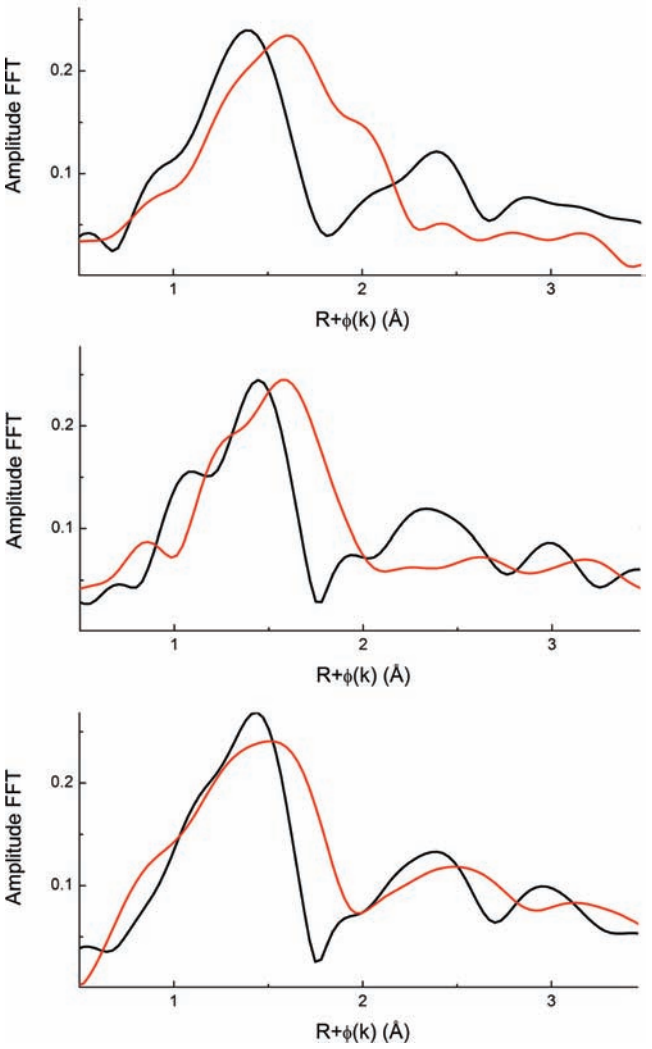

Figure 10. Fast Fourier transform of the k^2-weigthed EXAFS spectra for bulk $[Fe(Htrz)_2(trz)](BF_4)$ (top), sample **1** (center), and sample **2** (bottom) at 298 K (black line) and 397 K (red line).

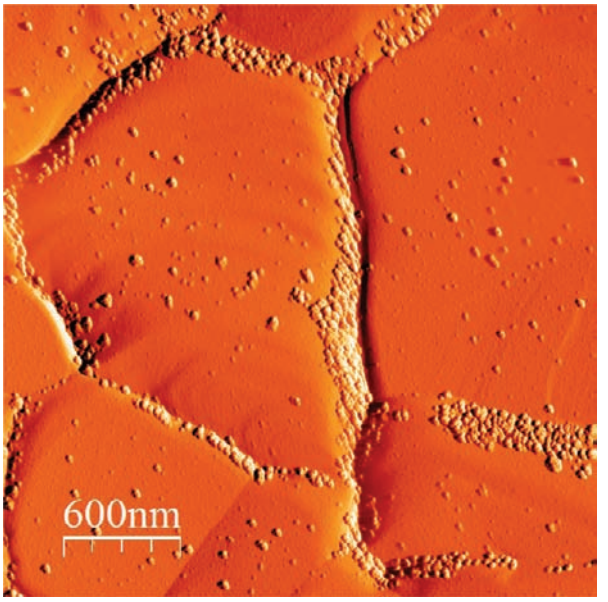

Figure 11. AFM image of nanoparticles of **1** on a gold substrate.

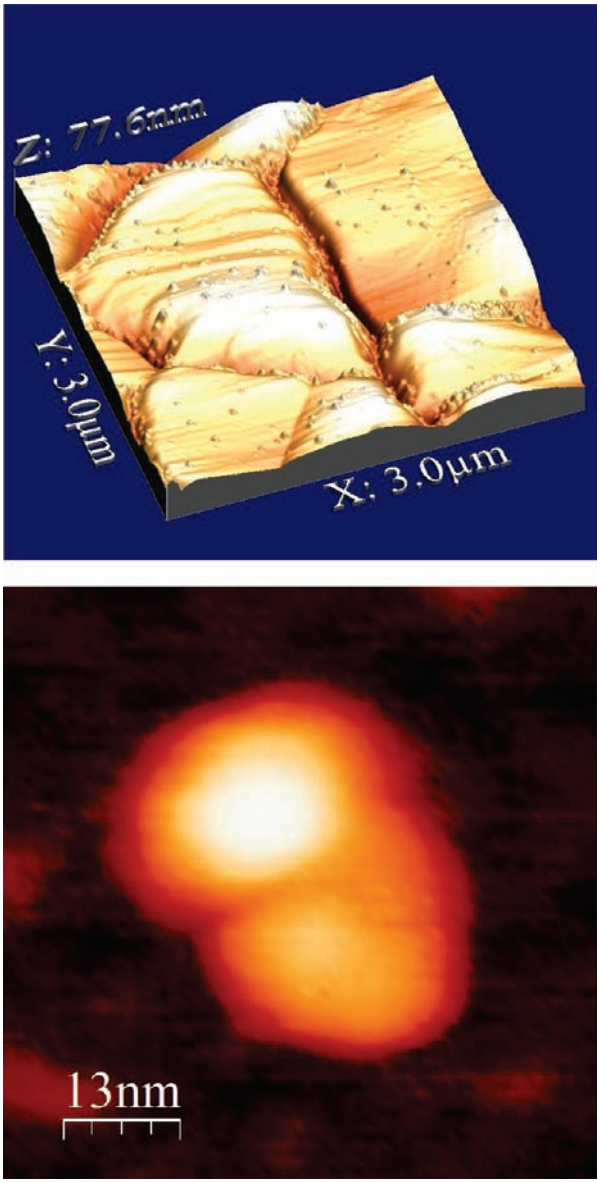

Figure 12. AFM high resolution topography image of nanoparticles of **1** on a gold substrate.

shows a different contrast for the nanoparticle core and the shell (Figure 14), giving us a clear look of the core and shell in these nanoparticles. We can also appreciate in these images that, in some cases, there are two individual nanoparticles inside one single organic shell. This suggests that the apparent dimerization we found on the previous AFM images on gold is probably not due to aggregation (aggregation hardly explains why we only found dimers, and not trimers or multiple groups of nanoparticles) but to the growth of two individual nanoparticles into one single organic shell.

Conclusions

We have demonstrated that spin crossover phenomena can be found in nanoparticles as small as 6 nm in size, showing spin transition with thermal hysteresis. The spin transition was followed by magnetic measurements, confirmed by EXAFS data and observed in the color changes of diluted suspensions of the nanoparticles. The synthetic process we have developed allows for the convenient preparation and

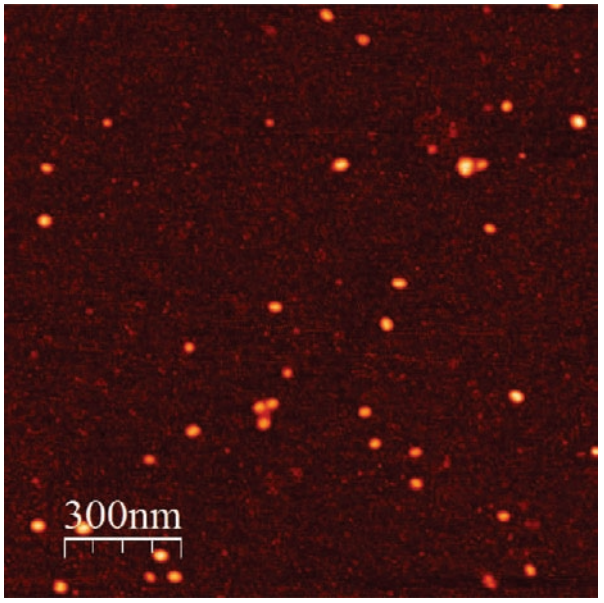

Figure 13. AFM image of single nanoparticles of **1** on a silicon substrate.

manipulation of these nanoparticles. The fact that the spin crossover phenomenon is retained at such small sizes opens the way for the implementation of these nanoparticles in ultra-high-density read/write device magnetic memories.

We have also shown how we can tune the spin transition temperature and hysteresis width by chemically changing the components of these nanoparticles. We were able to reach temperatures closer to room temperature. While sample **1** showed bistability above 60 °C, sample **7** shows bistability above 35 °C. These results reinforce that further chemical modifications could deliver bistable nanoparticles below 30 °C. This will obviously represent an advantage for actual technological applications. Still, it is noteworthy that hysteresis is about 30-K-wide in most samples, more than enough for information storage purposes.

In order to apply these nanoparticles into information storage devices or sensors, the next step is to organize them supramolecularly onto surfaces or other hosts for direct addressing and manipulation of such objects. The first steps in this direction have also been performed. We have shown how these nanoparticles, without further functionalization, can be deposited onto gold or silicon surfaces. We were able to study individual nanoparticles with AFM showing the organic shell that protects single domain cores of around 6 nm in size, responsible for the magnetic features. The next step will be to organize in a regular way these nanoparticles on surfaces. For this purpose, patterning techniques, as for example AFM local oxidation nanolithography or lithography controlled dewetting, which have been successfully applied to fabricate 2D nanostructures of molecular systems and nanoparticles with nanoscale accuracy, will be used.[30,31] And the final goal will be to investigate if the spin transition is still present in a single nanoparticle on a surface. This transition exists in suspension, but it is still unclear if it will remain unaffected for a single nanoparticle on a surface. The use of a spin-polarized STM as well as the study of the electron transport through a single nanoparticle are expected to clarify this point. This work is under way.

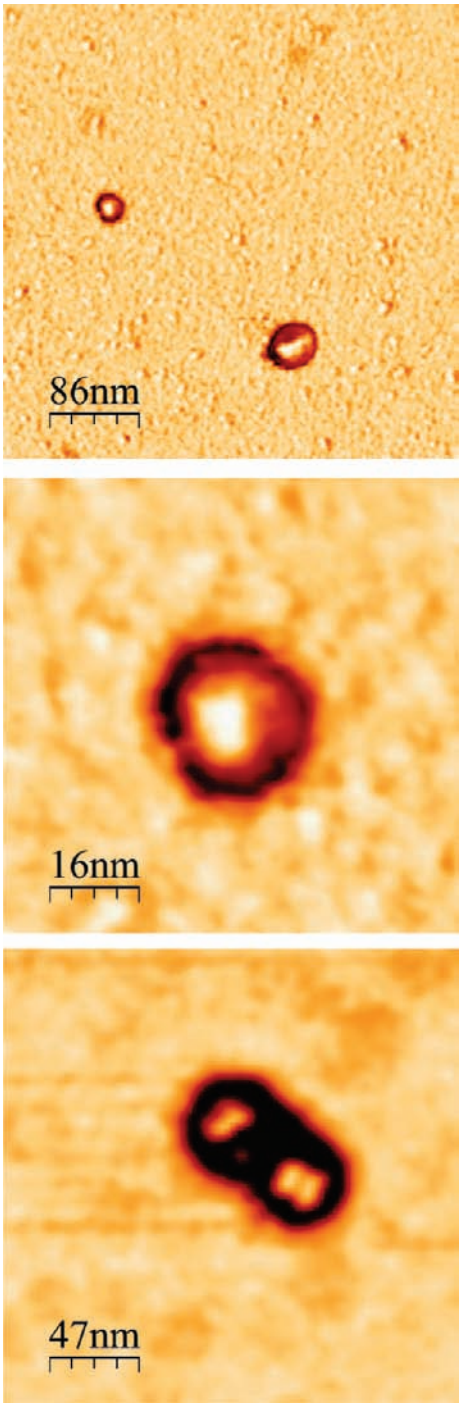

Figure 14. AFM high resolution phase images of single nanoparticles of **1** on a silicon substrate showing the difference between the core and the shell and the presence of dimerized units.

The spin crossover nanoparticles prepared and characterized by our groups show quite a different result when compared with those reported by other groups in analogous systems, where thermal hysteresis disappears below 20−30 nm size. This fact deserves some further commentary. Regarding those nanoparticles based in 3D systems, the difference in dimensionality can indeed be responsible for this effect. In the 3D systems, the size of the coordination polymer (responsible

(30) Garcia, R.; Magerle, R.; Perez, R. *Nat. Mater.* **2007**, *6*, 405–408.
(31) Martínez, R. V.; García, F.; García, R.; Coronado, E.; Forment-Aliaga, A.; Romero, F. M.; Tatay, S. *Adv. Mater.* **2007**, *19*, 291–295.
(32) Martínez, R. V.; Martínez, J.; Chiesa, M.; García, R.; Coronado, E.; Pinilla-Cienfuegos, E.; Tatay, S. *Adv. Mater.* **2010**, *22*, 588–589.

for the cooperative effect) is being reduced following an r^3 rate, while in a 1D system, as in the present case, the length of the chains is reduced following r. In 10 nm nanoparticles, we still have a longest chain length of about 20−25 iron centers. And the length is reduced to 10−12 iron centers for 6-nm-diameter nanoparticles. These results indicate that, in the family of $[Fe(trz)_3]_\infty$ materials, the cooperativity is essentially 1D. The apparently contradictory results reported for other 1D spin crossover nanoparticles are more puzzling, since the same reverse micelles technique was used in both cases. Still, we need to point out that the nanoparticles are based on a different compound (bromide vs tetrafluoroborate or perchlorate), and they followed a different stabilization process. There is no doubt that this subtle but important change must be responsible for the different outcome. Thus, it looks like that, for the moment, our preparative process and the materials selected by our research groups are indeed the most interesting prospect toward applications in molecular nanospintronics.

Acknowledgment. We thank the financial support from the European Union (Project MOLSPINQIP and ERC Advanced Grant SPINMOL), the Spanish Ministerio de Ciencia e Innovación (Project Consolider-Ingenio in Molecular Nanoscience and projects MAT2007-61584 and CTQ-2008-03197/BQU), and the Generalitat Valenciana (Prometeo Program). Partial financial support from Laboratorio Nacional de Luz Sincrotron, Campinas, Brazil, is also acknowledged. M.C. is a staff member of CONICET, Argentina. M.M.-C. thanks the MICIN for a predoctoral fellowship. A.F.-A. thanks the MICIN for a *Juan de la Cierva* contract.

Supporting Information Available: Dynamic light scattering, XAS, and EXAFS data are available. A real time movie with the heating−cooling cycle of a suspension of **1** in *n*-octane is also included. This material is available free of charge via the Internet at http://pubs.acs.org.